JACS
JOURNAL OF THE AMERICAN CHEMICAL SOCIETY

Article

Bisphosphonate-Generated ATP-Analogs Inhibit Cell Signaling Pathways

Satish R. Malwal, Bing O'Dowd, Xinxin Feng, Petri A. Turhanen, Christopher J. Shin, Jiaqi Yao, Boo Kyung Kim, Noman Baig, Tianhui Zhou, Sandhya Bansal, Rahul L. Khade, Yong Zhang, and Eric Oldfield

J. Am. Chem. Soc., **Just Accepted Manuscript** • DOI: 10.1021/jacs.8b02363 • Publication Date (Web): 22 May 2018

ACS Publications

is published by the American Chemical Society. 1155 Sixteenth Street N.W., Washington, DC 20036

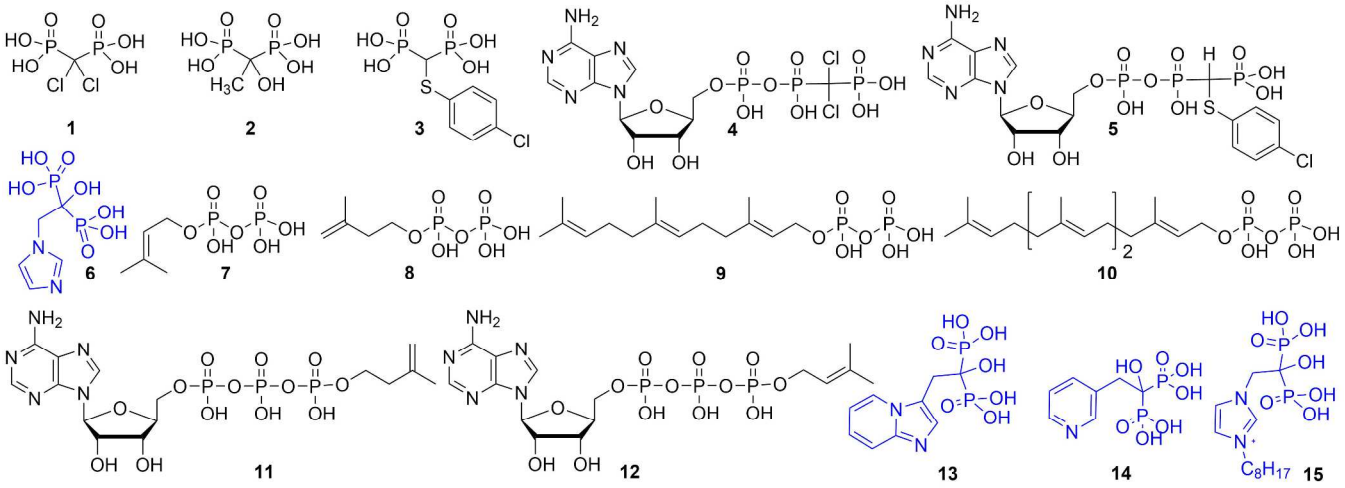

Figure 1. Structures of compounds discussed in the text. NBP's are shown in blue.

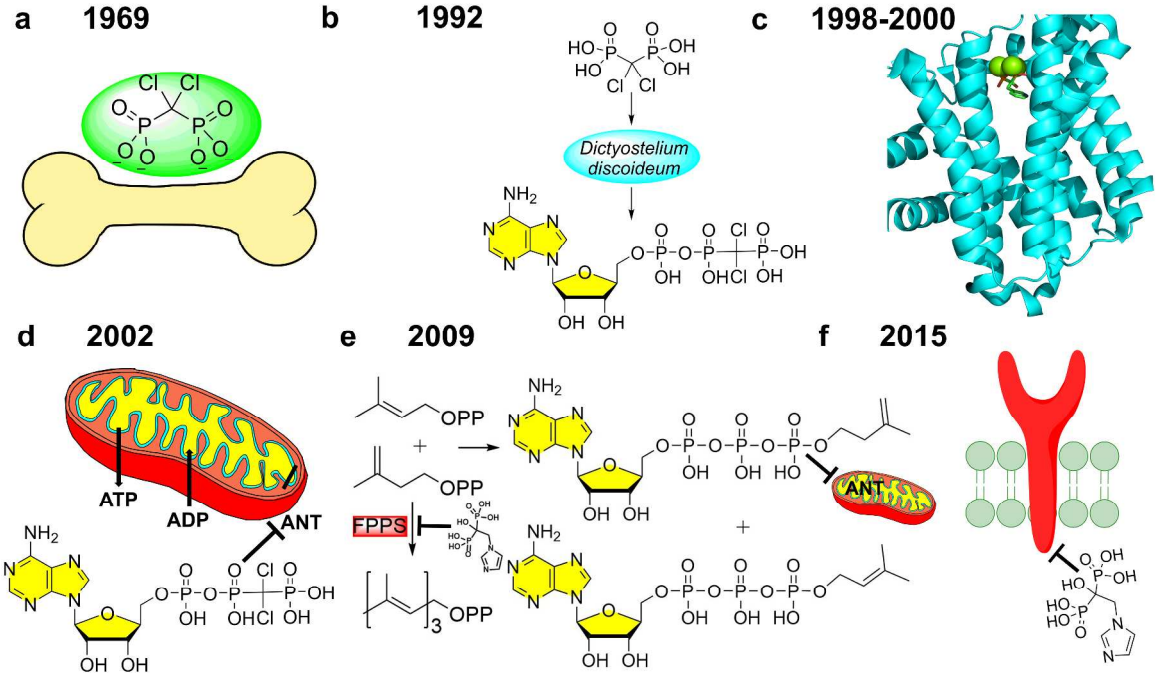

Figure 2. Time-line for proposed bisphosphonate mechanisms of action. (a) In 1969, clodronate and etidronate were proposed to affect bone resorption by a "physical" mechanism, involving direct bone-binding, inhibiting hydroxyapatite dissolution. (b) In 1992, clodronate and etidronate were shown to be converted to ATP analogs, AppXp, in the slime mold *Dictyostelium discoideum*, a model for osteoclasts. (c) In 1998-2000, next generation NBPs such as risedronate were shown to block protein prenylation by inhibiting farnesyl diphosphate synthase. (d) In 2002, it was shown that AppCCl$_2$p inhibited the mitochondrial adenine nucleotide translocase (ANT). (e) In 2009, it was shown that NBPs such as zoledronate led to accumulation of isopentenyl diphosphate and dimethylallyl diphosphate which were then converted to ApppI and ApppD, with ApppI being found to inhibit the ANT. (f) In 2015, it was reported that NBPs such as risedronate and zoledronate could act by directly inhibiting the epidermal growth factor receptor (EGFR).

Figure 2f. There was, however, a puzzling "dose discrepancy" between the effects of bisphosphonates in cell-free systems (IC$_{50}$ ~500 μM in EGFR inhibition assays) *versus* cell-based assays (EC$_{50}$ ~50 μM), in tumor cell killing,[20 21] and the 500 μM value for EGFR inhibition is ≈5-6 orders of magnitude larger than that found with conventional EGFR inhibitors. We thus sought to deduce models for bisphosphonate activity that might help explain these previous observations. We tested three hypotheses: First, NBPs do not directly inhibit the EGFR. Rather, the ATP analogs **11** and **12** are the kinase inhibitors, because these compounds have structural similarity to ATP. Second, with NNBPs such as clodronate, we hypothesized that ATP-analogs such as AppCCl$_2$p (**4**; adenosine 5'-(beta, gamma-dichloromethylene) diphosphate) also inhibit kinases. Third, we hypothesized that if species such as AppCCl$_2$p inhibited kinases, then lipophilic "pre-prodrug" forms of the NNBPs[22-24] might act by inhibiting cell signaling

Table 1. IC_{50} values for EGFR inhibition by bisphosphonates, phosphonate-containing ATP analogs, and known inhibitors

Compounds	IC_{50}(μM)
erlotinib	(3.8±0.25) x10^{-4} (n=2)
staurosporine	0.026±0.008 (n=6)
AppCCl_2p (**4**)	0.64±0.13 (n=3)
ApppI (**11**)	9.2±4 (n=6)
ApppD (**12**)	14
minodronate (**13**)	30
AMP-PNP	36
tiludronate (**3**)	43±12 (n=2)
zoledronate (**6**)	72±12 (n=2)
risedronate (**14**)	97
BPH-1222 (**15**)	100
alendronate	220
N-(2-(3-picolyl)AMDP	300
ibandronate	430
pamidronate	690
etidronate (**2**)	740

Table 2. Top 20 hits from 369 kinase screens with AppCCl_2p (4) and ApppI (11)[a]

Kinase (+**4**)	IC_{50} (μM)	Kinase (+**11**)	IC_{50} (μM)
JAK3	1.5E^{-03}	EGFR	1.0
PDGFRa	0.01	MST4	1.5
JAK2	0.02	TYK1/LTK	1.5
FGFR2	0.05	CDK7/cyclin H	1.6
DDR2	0.08	Aurora B	1.8
ABL1	0.09	SGK3/SGKL	2.4
PKCepsilon	0.09	PLK1	2.6
JAK1	0.10	NEK7	2.7
FRK/PTK5	0.11	ERBB4/HER4	2.7
RET	0.12	DLK/MAP3K12	3.4
FLT3	0.12	ULK3	3.4
PKCd	0.14	ASK1/MAP3K5	3.4
LYN B	0.21	ERN1/IRE1	3.5
ABL2/ARG	0.21	NEK1	3.9
EGFR	0.21	PKCtheta	3.9
DYRK3	0.22	P38d/MAPK13	4.0
JNK2	0.23	ROS/ROS1	4.0
TYK2	0.23	STK25/YSK1	4.1
FGFR1	0.24	GSK3b	4.3
c-MET	0.25	YSK4/MAP3K19	4.3

a) Pink = Tyr kinase; Cyan = Ser/Thr kinase

pathways. We tested these hypotheses using results for a broad range of NBPs and NNBPs, AppXp ATP-analogs (where X is a variable group that bridges Pβ and Pγ) and AppXp pre-prodrugs in, as appropriate, kinome screens with 369 kinases, 47 individual kinase dose response assays, cell growth inhibition assays using 6 cell lines, Western blots, mitochondrial respiration assays, FPPS and GGPPS inhibition, ApppI formation assays, as well as geranylgeraniol (GGOH) "prenylation rescue" assays.

RESULTS AND DISCUSSION

Bisphosphonates are not potent EGFR inhibitors. We first investigated the effects of 11 bisphosphonates (8 NBPs and 3 NNBPs) on EGFR inhibition using a wild type EGFR kinase-domain assay, with poly[Glu:Tyr](4:1) and [γ-^{33}P]-ATP as substrates. Dose-response curves are shown in Figure S1 and numerical values are summarized in Table 1. The IC_{50} values were many orders of magnitude higher than we find with the known EGFR inhibitors staurosporine (IC_{50}=26± 8 nM; n=6) or erlotinib (IC_{50}~380 ± 250 pM; n=2), ranging from ~30-40 μM (minodronate **13**, tiludronate **3**) to ~70-100 μM (zoledronate **6**, risedronate 1**4** and a lipophilic bisphosphonate, **15**,[25] to >100 μM for alendronate, N-(2-(3 picolyl)aminomethylene bisphosphonate, ibandronate, pamidronate, etidronate and clodronate, Table 1, showing that inhibition of the EGFR by many bisphosphonates is very weak. In contrast, we found that the ApppI that accumulates in cells on FPPS inhibition inhibited EGFR kinase activity with an IC_{50} of 9.2 ± 4 μM (n=6). Dose-response curves are shown in Figure S1. So, ApppI is a more potent EGFR inhibitor than any of the bisphosphonates tested, or indeed the ATP analog AMP•PNP, which has an IC_{50} of 36 μM in this assay. We also prepared and tested the dimethylallyl ester of ATP, ApppD (**12**)[26-27] finding an IC_{50}~14 μM (Figure S1).

ApppI has been reported to accumulate in some cells to >100 μM levels, on bisphosphonate treatment[15]. However, given typical ATP concentrations in cells (~1-5 mM) and known K_M [ATP] values (~5 μM[28]), it seems that EGFR inhibition by **11** or **12** will not be a major target for cell growth inhibition. In contrast, we found much more potent EGFR inhibition with AppCCl_2p (IC_{50}=640±120 nM), Figure S1, of interest since AppCCl2p levels in some cells can reach mM levels.[15, 29] We thus find that bisphosphonates do not directly inhibit the EGFR in the same assays in which we obtain potent, low nM inhibition by the known kinase inhibitors, staurosporine and erlotinib. But the results do suggest the possibility that some ATP-analogs might potently inhibit this or other kinases—indicating the desirability of a large kinome screen.

Kinome-screening results for AppCCl_2p and ApppI. To see whether any kinases were potently inhibited by AppCCl_2p or ApppI, we carried out screens of 369 kinases using the HotSpot℠ assay (Reaction Biology Corporation; 20 mM Hepes, pH 7.5, 10 mM $MgCl_2$, 1 mM EGTA, 0.02% Brij-35, 1 μM ATP, single dose duplicate mode at 1 μM inhibitor) using both compounds. Results (computed IC_{50} values) are shown in Table 2 for the top 20 hits and complete kinome screen results are in Tables S1 and S2. In order to obtain more accurate results, we then carried out a series of 10-dose, dose-response assays for ApppI (8 kinases; Figure S2) and AppCCl_2p (17 kinases, Figure S3). For the 17 kinases where we obtained both dose-response as well as kinome screen results we found a Pearson R-value correlation coefficient R=0.96 between the IC_{50} values for the two data sets (Figure S4).

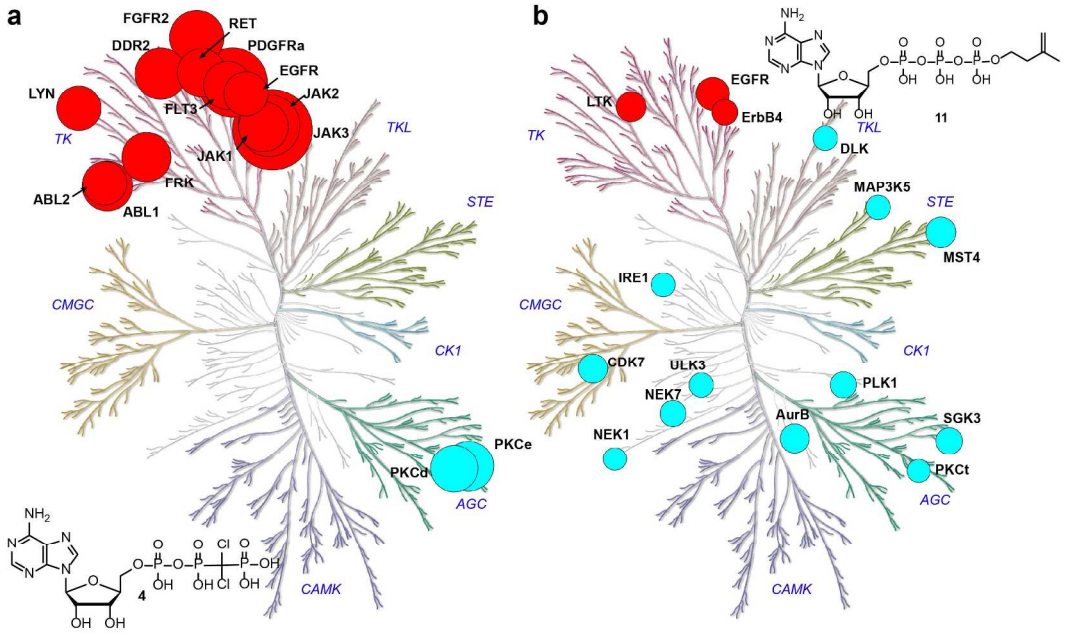

Figure 3. Kinase inhibition results for $AppCCl_2p$ (**4**) and ApppI (**11**) mapped onto a Kinmap dendrogram showing more potent and selective Tyr-kinase inhibition by $AppCCl_2p$. (a) Kinmap dendrogram for $AppCCl_2p$. (b) Kinmap dendrogram for ApppI. The size of the circle was set in Kinmap as 100+(50*pIC_{50} [μM]) so the larger the circle, the lower the IC_{50}. Red = Tyr kinase; Cyan = Ser/Thr kinase. $AppCCl_2p$ inhibits almost exclusively Tyr-kinases but ApppI inhibits a broader range of kinases, albeit only weakly.

What the results in Tables 2 and 3 show is that there is potent (~10s nM) inhibition of several kinases (e.g. PDGFRα, JAK2, JAK3, FGFR2) by $AppCCl_2p$, plus, many other kinases are inhibited at higher concentrations. Moreover, for JAK3 we determined K_i values at 1 μM and 200 μM ATP levels and using reported K_M ATP values[30] we find K_i ~ 4-11 nM. However, the inhibitory effects of ApppI and AppD (ApppD dose-response curves for 9 kinases shown in Figures S1 and S5) are very much weaker. These results have several implications. First, since $AppCCl_2p$ levels in clodronate-treated macrophages can reach mM levels[29] and ApppI can reach ~130 μM[15] (and ApppD is ~2x higher), numerous kinases will be inhibited although the effects will be much more pronounced with clodronate/$AppCCl_2p$ because the IC_{50} values there are ≈2-3 orders of magnitude smaller than with ApppI/ApppD. Second, it has recently been shown[31] in mice breast cancer models (as well as in one patient) that bisphosphonates bind to granular micro-calcifications that are then engulfed by tumor-associated macrophages (TAMs). This is expected to lead to high $AppCCl_2p$ levels in TAMs and as noted by Junankar et al.,[31] TAMs are powerful promoters of tumor growth and meta stasis,[32] and extensive macrophage infiltration in many tumor types is associated with poor patient prognosis".[33] It thus appears that some of the extra-skeletal effects of bisphosphonate therapy especially with breast cancer patients could arise from kinase inhibition in TAMs. In mice treated with NBPs, ApppI levels in osteoclasts reach ~20 μM,[34] so direct kinase inhibition is unlikely to be a major contributor to activity. Third, clodronate levels in tissues in patients on systemic clodronate therapy are expected to be low because bisphosphonates bind avidly to bone mineral but intriguingly, there are several reports of the anti-inflammatory effects of NNBPs[35-42] so our finding that JAK 1/3 and Tyk2 are some of the kinases that are inhibited by $AppCCl_2p$ is of interest since the anti-inflammatory drug Xeljanz® functions by inhibiting JAK 1/3,[43-44] and we find a 5 nM IC_{50} for JAK3 inhibition (and as discussed below, STAT3 involvement in activity with an AppXp analog). Fourth, we see that FGFR2 (the fibroblast growth factor 2 receptor) is inhibited by $AppCCl_2p$ (IC_{50} ~22 nM) and in earlier work[45] it was shown that clodronate reduced FGF2-driven cell growth in HUVECs (human umbilical vein endothelial cells), but there was no effect in the absence of FGF2. In that work it was proposed that clodronate bound directly to FGF2, inhibiting its activity, but here, we now have evidence for low nM FGFR2 inhibition by $AppCCl_2p$, suggesting a direct effect of the clodronate metabolite on FGFR2 cell signaling. Overall then, the kinase inhibition results reveal that there are multiple kinases that are quite potently inhibited (IC_{50} ~ 10s nM) by $AppCCl_2p$, offering new insights into the mechanisms of action of the clodronate.

$AppCCl_2p$ and ApppI target different kinase classes. When all of the kinase inhibition results are examined it is apparent that there are four trends that relate to tyrosine versus serine/threonine kinase inhibition by $AppCCl_2p$ and ApppI, and kinase inhibition in general. First, the targets for $AppCCl_2p$ and ApppI are different. For the 20 most potent "hits" in the kinome screens, $AppCCl_2p$ targets ~78% tyrosine kinases, highlighted in pink in Table 2, but only 22% of the top 20 are serine/threonine kinases, highlighted in cyan in Table 2. Second, only ~14% of the top 20 hits in the ApppI kinome screen are tyrosine kinases but ~86% of the top 20 are serine/threonine kinases, Table 2. Third,

the activities of AppCCl$_2$p and ApppI when mapped onto kinome dendrograms (using the Kinmap program[46]) (Figure 3a, 3b) clearly show that the vast majority of AppCCl$_2$p targets are in the TK (tyrosine kinase) group, while ApppI inhibition is much more widespread and as noted, favors Ser/Thr kinases. Fourth, AppCCl$_2$p is a much more potent kinase inhibitor than is ApppI (or ApppD). What, then, might be the molecular basis for the differential effects (on both activity and selectivity) of AppCCl$_2$p and ApppI?

A molecular basis for AppCCl$_2$p activity and selectivity. The more potent and selective activity of AppCCl$_2$p for Tyr versus Ser/Thr kinases could be due to stronger binding to Tyr kinases in general, model A, or to stronger binding to Tyr versus Ser/Thr OH groups in substrates, model B. The latter model is attractive since the phosphonate group in AppCCl$_2$p would be expected to form a much stronger hydrogen bond with the aromatic Tyr than with the aliphatic Ser/Thr. This is because, as shown in Figure 4a, there can be strong hydrogen bonding between phosphonate/phenol and phosphonic acid/phenolate species that cannot occur with Ser/Thr due to the very high pK_a values (~16) of aliphatic alcohols. These sorts of hydrogen bonds are well known in e.g. salicylates in which the carboxylate interacts with a phenolic OH.[47]

We thus next used a LanthaScreen Eu kinase binding assay with activated JAK3 to determine (in the absence of substrate) the K_i for AppCCl$_2$p binding. We found K_i=73 nM (Figure S6) which is much higher than the K_i ~4-11 nM found in the activity assays (at 1 and 200 μM ATP). This means that the presence of a substrate Tyr is required for high affinity binding, supporting model B. Then, to test if phosphonate-tyrosine hydrogen bond interactions are indeed significantly different to phosphonate-serine/threonine interactions, we used density functional theory (DFT) and Atoms-in-Molecules (AIM) theory.[48]

AIM theory is a quantum chemical method that we and others have used to investigate the details of hydrogen bond interactions.[49] According to AIM theory, every chemical bond has a bond critical point (BCP) at which the first derivative of the charge density, ρ(**r**), is zero. The ρ(**r**) topology is described by a real, symmetric, second-rank Hessian-of-ρ(**r**) tensor, and the tensor trace is related to the bond interaction energy by a local expression of the virial theorem:

$$\mathrm{Tr(Hessian)} = \nabla^2\rho(\mathbf{r}) = [2G(\mathbf{r}) + V(\mathbf{r})]\ (4m/\hbar^2) \qquad (1)$$

where $\nabla^2\rho(\mathbf{r})$ is the Laplacian of (**r**), and G(**r**) and V(**r**) are electronic kinetic and electronic potential energy densities, respectively. Negative and positive $\nabla^2\rho(\mathbf{r})$ values are associated with shared-electron (covalent) interactions and closed-shell (electrostatic) interactions, respectively. In the latter case, one can further evaluate the total energy density, H(**r**), at the bond critical point:

$$H(\mathbf{r}) = G(\mathbf{r}) + V(\mathbf{r}) \qquad (2)$$

A negative H(**r**) is termed partial covalence, while a positive H(**r**) indicates a purely closed-shell, electrostatic interaction[50]. We first used the models shown in Figure 4b to examine the differences in the interactions between a

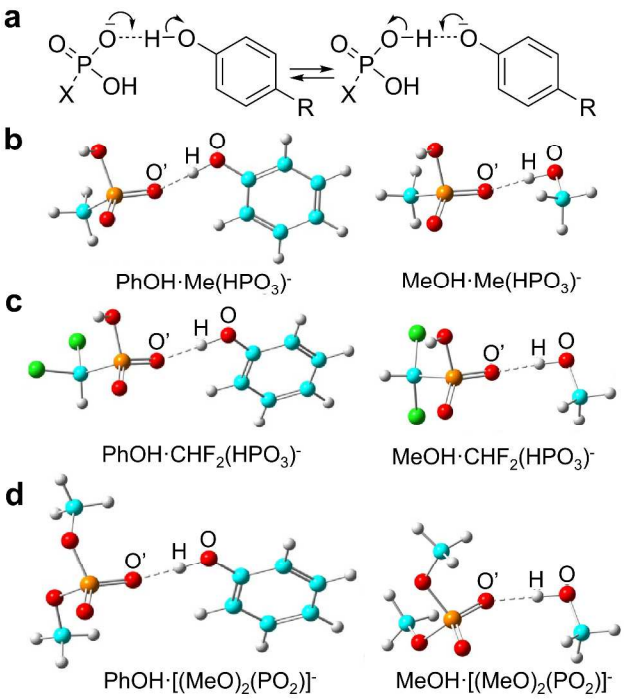

Figure 4. Schematic illustration of hydrogen bonding of phenol/phosphonate, and geometry-optimized structures. (a) A phenol/phosphonate hydrogen bond. (b) Geometry-optimized structures of phenol or methanol with methyl phosphonate. (c) As (b) but phenol or methanol with difluoromethyl phosphonate. (d) Phenol or methanol with a dimethyl phosphate. Geometries, bond critical point values and predicted ^{1}H NMR shifts are in Table S3.

bisphosphonate (modeled here as Me(HPO$_3$)$^-$) and Tyr (modeled as PhOH), *versus* with Ser/Thr (modeled as MeOH). The optimized geometries for PhOH·Me(HPO$_3$) and MeOH·Me(HPO$_3$)$^-$ are quite similar (Figure 4b and Table S3.). As shown in Table S3, the hydrogen bond in the Tyr (phenol) model system is clearly stronger, as indicated by a 0.115 Å shorter O'...H distance and a 0.096 Å shorter O'...O distance. AIM-calculated BCP properties show that the OH bonds in PhOH and MeOH are of a covalent nature, having large negative Laplacians. However, the O'...H hydrogen bonds in both systems are by definition of a closed-shell (electrostatic) nature, since they have positive Laplacians. They also exhibit what is called partial covalence, due to a negative H(**r**), which is 230% larger in the Tyr than in the Ser/Thr model system. The charge densities ρ(**r**) and electronic kinetic and potential energy densities G(**r**) and V(**r**) are also larger (30-45%) in the hydrogen-bond in the Tyr versus Ser/Thr model system, meaning a stronger H-bond with the Tyr model. To help confirm this, we carried out two additional sets of calculations, using a difluoromethylene phosphonate CHF$_2$(HPO$_3$)$^-$ to model AppCCl$_2$p, and [(MeO)$_2$PO$_2$]$^-$ to model ApppI. The optimized structures are shown in Figure 4c and 4d. All computed properties were very similar to those found with the initial models (Table S3), confirming that the phosphonate hydrogen bond in the Tyr model is much stronger than in the Ser/Thr model. An atomic charge analysis shows that the charge on PhOH in the complexes is ~65% more

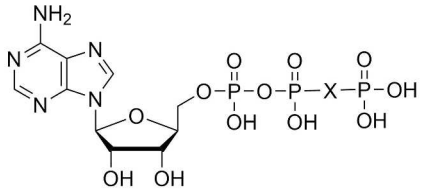

16, **X**=CH_2; **17**, **X**=CHF; **18**, **X**=CF_2; **19**, **X**=CFCl; **20**, **X**=CFBr; **21**, **X**=$CMeN_3$; **22**, **X**=CClBr; **23**, **X**=CBr_2; **24**, **X**=$CHOC_6H_4$-*p*-Cl; **25**, **X**=$CHCH_2C_6H_3$-*m*,*p*-Br_2; **26**, **X**= $CHSC_6H_3$-*m*,*p*-Br_2

Figure 5. Structures of AppXp analogues synthesized.

negative than that for MeOH, due to the stronger ability of the phenyl ring to delocalize charge from the $Me(HPO_3)^-$ or $CHF_2(HPO_3)^-$ species, providing in essence, additional resonance stabilization that again contributes to a stronger interaction with Tyr.

Another way to view these interactions is to consider the ^{1}H NMR chemical shifts of the protons involved in hydrogen bonding (Table S3), as we have reported previously,[47, 49] in which partial covalence occurs when ^{1}H NMR shifts in hydrogen bonded systems reach the 12-14 ppm range (downfield from TMS), while fully shared-electron (covalent) interactions have shifts of ~21 ppm.[49] With the Tyr models, the computed chemical shifts (~12-13 ppm) are much larger than those of the proton involved in the hydrogen bond in the Ser/Thr model (~6-7 ppm), consistent with the onset of partial covalence, and these ~12-13 ppm shifts are very similar to those we have found in intra-molecular hydrogen bonds in salicylates.[47] So: the Tyr versus Ser/Thr selectivity effects seen with $AppCCl_2p$ are consistent with stronger hydrogen bonding to Tyr, which we compute to be ΔE ~3.9 kcal mol^{-1} larger than in the Ser/Thr model. A frequency analysis was then used to verify the nature of the stationary points on the respective potential energy surfaces, yielding a $\Delta\Delta G$ (at 300 K, 1 atm) of 2.85 kcal mol^{-1}, corresponding to a ~100x increase in binding to Tyr. With ApppI, kinase inhibition is very much weaker, likely due to steric repulsions of the bulky isopentenyl group with Tyr or Ser/Thr, an effect that would of course be largest with the more bulky Tyr.

Synthesis of novel AppXp analogs, and kinase inhibition. Given that there are several kinases that are inhibited by $AppCCl_2p$, the question arises: can more potent species be developed? In the case of bone resorption, the NBP zoledronate is a very effective drug, but there are numerous cases of bisphosphonate-related osteonecrosis of the jaw and it has been suggested that new NNBPs with anti-inflammatory activity might help decrease this risk.[40] The anti-inflammatory activity of NNBPs is also of interest given their potent JAK2 and JAK3 inhibition, plus, tiludronate has been shown to reduce cytokine production from activated macrophages,[35] to alleviate cachexia in nude mice xenograft models,[38] and is reported to be effective in treating erosive osteoarthritis of the hand[41] as well as knee osteoarthritis[39] effects that might all be improved with more active/bioavailable species. Plus, in the case of anti-cancer activity, kinases might also be targets for NNBP pre-prodrugs[22-24] that form AppXp inhibitors. For example, we find that the activity of $AppCCl_2p$ against wild type EGFR is

Table 3. Dose-response IC_{50} values for $AppCCl_2p$ inhibition of 18 kinases[a]

Kinase	IC_{50}	Kinase	IC_{50}
PDGFRa	4 nM	FRK/PTK5	100 nM
JAK3	5 nM	RET	140 nM
JAK2	13 nM	EGFR (T790M)	270 nM
FGFR2	22 nM	EGFR (L858R)	490 nM
PKCepsilon	43 nM	EGFR	560 nM
DDR2	47 nM	EGFR (G719S)	760 nM
JAK1	66 nM	EGFR (d746-750)	4.3 μM
ABL1	79 nM	BRAF	6.4 μM
EGFR (L858R, T790M)	80 nM	BRAF (V599E)	230 μM

a) Pink = Tyr kinase; Cyan = Ser/Thr kinase

IC_{50} ~250 nM, but against 5 mutants, we find d746-750, 4.3 μM; G719S, 760 nM; L858R, 490 nM; T790M, 270 nM; L858R, T790M, 80 nM, Table 3 and Figure S4.

Since $AppCCl_2p$ is a relatively potent inhibitor of the L858R, T790M double mutant and since this an important drug target, we elected to synthesize a series of $AppCCl_2p$ analogs and test them against the EGFR, as well as against the L858R, T790M mutant. We synthesized 8 analogs (**16**-**23**; Figure 5) containing small substituents at the carbon bridging Pβ and Pγ, as well as 4 analogs (**5**, **24**-**26**) containing larger, aryl substituents. The dibromobenzyl species **25** was of interest since the parent bisphosphonate esters were previously shown[22] to have potent activity against three human tumor cell lines. As with tiludronate, the "pro tected" dibromobenzyl ester bisphosphonate was convert ed in cells to the AppXp analog **25**, as shown in the MS and LC-MS results in Figures S7a and S7b. All EGFR inhibition dose-response curves are in Figures S8a, S8b, and IC_{50} values are in Table S4. The most potent EGFR inhibitors have CFCl, CCl_2, CBr_2, or $C(Me)N_3$ bridging groups between Pβ and Pγ, and there is a parabolic dependence of activity on the van der Waals' surface area of the molecules (Figure S9a). There is also a strong correlation between the pIC_{50} values for EGFR versus EGFR (L858R, T790M) inhibition for n = 13 compounds, with an R = 0.96 (Figure S9b), the most active compounds (**23**) being the dibromo-analog of clodronate and (**21**) the methyl-azide, which inhibit the double mutant with IC_{50} values of 16 nM and 4 nM, respectively.

The results shown in Table S4 and Figure S9a indicate that there are several contributors to EGFR inhibition by these AppXp species. The most potent inhibitors have highly electron-withdrawing substituents on the bridging carbon. This results in a pK_a4 of 7.0 for $AppCCl_2p$,[51] essentially the same as the 7.1 found with ATP,[51] while the pK_a4 of the CH_2 analog **16** is 8.4, meaning qualitatively that protein electrostatic interactions with $AppCCl_2p$ will mimic those found with the ATP substrate. Plus, the phosphonate (O^-)...HO (Tyr) interaction will be favored (at least, at pH~7). Why then are some AppXp inhibitors better than others? What the parabolic dependence of IC_{50} on van der Waals' surface area shows is that activity initially increases with the size of the bridging carbon substituents, with the $CMeN_3$ and CBr_2 species having most activity, presumably

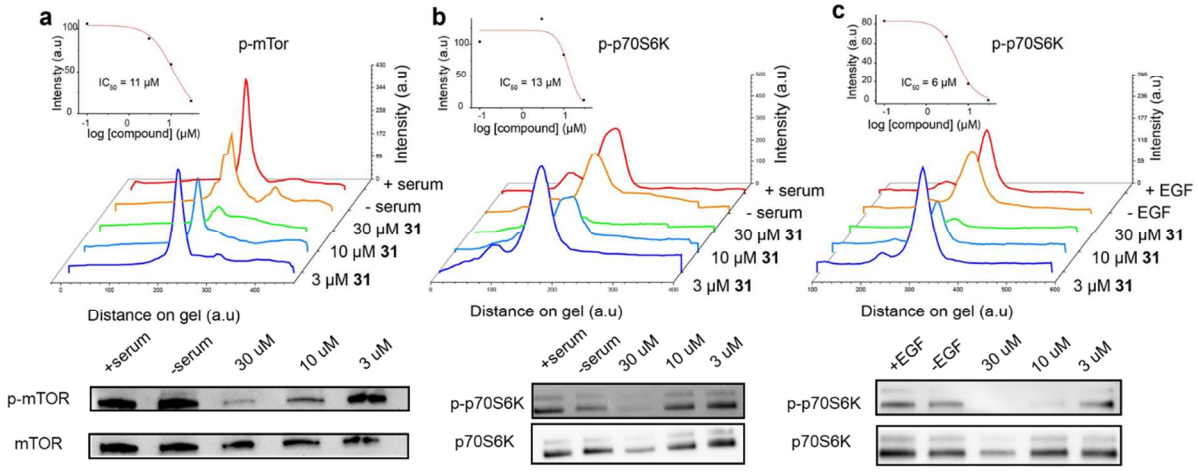

Figure 6. Western blot results for effects of **31** on mTOR and p70S6K phosphorylation. The stacked plots are summed photo-densitometer traces; representative gels are shown below, and dose-response curves and IC_{50} values (from summed intensities of 3 blots) are shown in the insets. (a) mTOR in MCF7 cells induced with serum. (b) p70S6K in MCF-7 cells induced with serum. (c) p70S6K in MCF-7 cells induced with EGF.

due to increased hydrophobic interactions. However, on addition of a very large (aryl) substituent, activity decreases, due to the onset of steric repulsions with the protein in addition to changes in the pK_a4 values and decreased electrostatic/hydrogen bonding interactions. Consistent with the EGFR inhibition results, we find low activity with both the tiludronate and dibromobenzyl analogs (**5**, **25**) in other kinase assays (Figures S10 and S11). The questions then arise: what activity do the parent bisphosphonate prodrugs, as well as pre-prodrug analogs, have in cells?

Cell and organelle activity of NNBPs, AppXps, and AppXp pre-prodrugs. We next sought to see how the clodronate-analog bisphosphonates and their pre-prodrug forms **27**-**33** (Figure S12) inhibited tumor cell growth, as well as how the corresponding AppXp analogues inhibited the ANT (as measured *via* mitochondrial respiration). The smaller bisphosphonates had very poor cell (H460) growth inhibition activity, with IC_{50} values of ~500 μM. This improved with the addition of an aromatic side-chain, the dibromobenzyl bisphosphonate having an IC_{50}~26 μM. However, major increases in activity were only found with the pre-prodrug species (**27**-**33**), as shown in Figure S12, with the pivaloyloxymethylene (Piv) esters and the phosphoramidate analogs of clodronate[23-24] all having IC_{50} values in the 0.4-6 μM range. But how do the protected NNBPs–that is, their AppXp products actually kill cells?

It has been generally thought that the AppXp analogs of the NNBPs target the ANT, the adenine-nucleotide translocase, with Lehenkari et al.[14] reporting that the ANT was inhibited by $AppCCl_2p$ with an IC_{50} of ~50 μM and that mitochondrial respiration was likewise inhibited. We thus tested each of the 13 AppXp analogs as well as ApppI in a heart mitochondrial O_2-consumption assay: results are shown in Figure S13. The range in IC_{50} values was small 0.76 to 6.4 μM (Figure S13), and since concentrations of $AppCCl_2p$ in treated cells are typically in the 100s μM range, then ANT inhibition of mitochondrial respiration is clearly one target for all of the NNBP pre-prodrugs. However, in some cases, effects on respiration may be minor when compared with effects on kinase inhibition.

Scheme 1. Conversion of the pre-prodrug **31** to **23**.

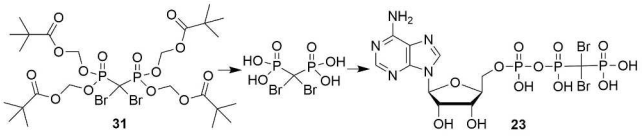

Western blot evidence for effects on cell signaling pathways. We next sought to determine whether the Piv-ester of the dibromo analog of clodronate, **31**, had any effects on cell signaling pathways since **31** was a potent NNBP pre-prodrug and its product **23** (Scheme 1, Figure S14) was a 100 nM EGFR inhibitor (Table S4). We began by screening for effects on cell signaling pathways in MCF-7 cells because MCF-7 is a high producer of $AppCCl_2p$ from clodronate. Since it seemed possible that multiple kinases and pathways might be targeted, we elected to first investigate the downstream proteins mTOR and p70S6K, chosen because of their central role in many signaling pathways, including osteoclast survival,[52] using Western blots. As can be seen in Figures 6a-6c, the Western blot results in MCF-7 cells show inhibition (IC_{50}~6-13 μM) of mTOR and p70S6K phosphorylation, so the NNBP pre-prodrug **31** (active metabolite $AppCBr_2p$, **23**) does affect signaling pathways in MCF-7 cells (which have a low EGFR copy number).

Next, since our initial idea was that the EGFR might be targeted by AppXp compounds, we investigated the EGFR pathway in A431 cells, chosen because EGFR is highly expressed. There was little effect of **31** on the autophosphorylation of EGFR, so we hypothesized that there might be involvement of other kinases (that we previously found were potently inhibited by $AppCCl_2p$ *in vitro*) and chose to investigate the phosphorylation of STAT3 (Signal Transducer and Activator of Transcription 3; Figure S15). STAT3 is involved in cell growth and apoptosis and is phosphorylated by Janus kinases (JAK) and as noted above, we found potent inhibition of JAK1, JAK2 and JAK3 by $AppCCl_2p$ (Table 2). As can be seen in Figure S15, there is again a dose-dependent inhibition (IC_{50}~7 μM) of STAT3 phosphorylation by **31**, as found also with clodronate itself

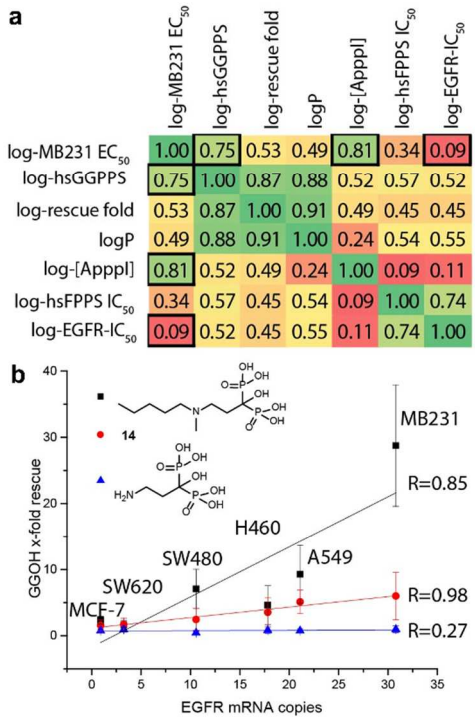

Figure 7. Correlations between cell growth inhibition and various properties, and GGOH-rescue results with three bisphosphonates in different cell lines. (a) Correlation between MD-MBA-231 cell growth inhibition pEC_{50} (=-$\log_{10}$ EC_{50} [μM]) and GGPPS inhibition pIC_{50}; GGOH rescue factor (the ratio of the EC_{50} with or without 20 μM GGOH); clogP; $\log_{10}$[ApppI; μM]; FPPS inhibition pIC_{50} and EGFR pIC_{50}. The numbers shown in the matrix are the Pearson R-value correlation coefficients. Green colors highlight strong correlations, yellow are intermediate, red indicates no significant correlation. (b) GGOH x-fold rescue of the growth inhibition of 6 cell lines for three bisphosphonates as a function of EGFR copy number. The R-values for two bisphosphonates are high but for pamidronate is not significant. The high correlation between cell growth inhibition and GGPPS inhibition (R=0.75) in (a) is very similar to that seen previously with MCF-7 cells and other bisphosphonates (R=0.80). The correlation between cell growth inhibition and ApppI levels is also very high (R=0.81) and taken together these results indicate the importance of multi-targeting with both protein geranylgeranylation as well as ApppI/AppppD inhibitors contributing to bisphosphonate activity.

in macrophages albeit at a higher inhibitor concentration.[53] So, the NNBP pre-prodrug **31** (and likely the other analogs) can affect both upstream (STAT3) as well as downstream (mTOR/p70S6K) signaling pathways, consistent with inhibition of one or more kinases.

Cell and organelle activity of NBPs: How do they work? The "standard model" for cell growth inhibition by NBPs has been that FPPS and/or GGPPS inhibition[54] leads to inhibition of protein prenylation, with ApppI formation and ANT inhibition also being of importance. More recently, NBPs have been reported to inhibit the EGFR, but there was a dose discrepancy between cell growth and kinase inhibition. To further probe the NBP mechanism of action, we investigated cell growth inhibition by the 8 NBPs listed in Table 1, compounds that inhibit GGPPS and/or FPPS, in a high-EGFR expressing cell line, MDA-MB-231. We measured growth inhibition activity (pEC_{50}=-$\log_{10}EC_{50}$[μM]; dose response curves in Figure S16), then correlated these effects with EGFR (Table 1), FPPS[54] and GGPPS[55] inhibition; GGOH growth inhibition rescue (Figure S16); ApppI accumulation (Figure S17), and with clogP, a measure of lipophilicity. Results are summarized in the Pearson R-value correlation matrix/heat map[54] shown in Figure 7a. There was essentially no correlation (R~0.09) between NBP-induced cell growth inhibition and EGFR inhibition. There was, however, a significant correlation between cell growth inhibition and ApppI levels, R=0.81, as well as with GGPPS inhibition, R=0.75, the GGPPS correlation being almost identical (R=0.8) to that we reported previously with a different set of bisphosphonates in a low EGFR expressing (MCF-7) cell line.[54] The observation that cell growth inhibition correlates with ApppI levels is in accord with the work of Mitrofan et al.[17] who reported that zoledronate-induced apoptosis correlated with high ApppI levels in three cell lines (MCF-7, MDA-MB-436 and RPMI 8226). The correlation with GGPPS inhibition supports a prenylation mechanism, while the ApppI correlation indicates an ANT mechanism, given that kinase inhibition is so weak. That is, there is strong evidence for multiple targeting. While it may seem surprising that we find a much better correlation between cell growth inhibition with GGPPS inhibition as opposed to FPPS inhibition this is precisely what we found previously with MCF-7 cells and a separate set of bisphosphonates,[56] with better cell activity being found with the more lipophilic NBPs such as **15** that have activity against both FPPS and GGPPS, as well as good cell penetration.

The observation that there are geranylgeraniol (GGOH) growth inhibition rescues with most NBPs has been taken to support a prenylation mechanism. Surprisingly though, Mitrofan et al.[17] noted that in some cells treated with zoledronate+GGOH (GGOH is converted in cells to GGPP), there was essentially no IPP/ApppI production a remarkable observation. They suggested that this might be due to negative-feedback regulating HMGCoA reductase activity[56-57] but an alternative or additional explanation for the lack of IPP/ApppI accumulation on zoledronate+GGOH treatment is that GGPP in addition to rescuing prenylation-inhibition is a potent (~60 nM) inhibitor of mevalonate kinase[58] whose inhibition will also block formation of isoprenoids. So, inhibiting mevalonate kinase and/or HMGCoAR activity will inhibit formation of ApppI and AppD, meaning that GGOH (or GGPP) can rescue cells from NBP growth inhibition in two ways: First, by providing GGPP for protein prenylation. Second, by blocking formation of ApppI/AppD.

The correlation between cell growth inhibition and GGPPS inhibition[54] indicates that there is a key role for protein geranylgeranylation in cell growth inhibition, as found previously with other cell lines[59-62], as does the observation that cell growth inhibition is rescued by addition of GGOH (Figure 7). Moreover, these "rescue" effects are dependent on the number of EGFR copies per cell (Figure 7b). In these experiments, we used MCF-7, SW620, SW480,

H460, A549 and MDA-MB-231 cell lines which have increasing EGFR copy numbers per cell.[63-66] We find a correlation between GGOH-rescue and EGFR copy number, most likely though an "indirect effect" due to large numbers of EGFR needing to interact with large numbers of prenylated Ras proteins to function as opposed to any direct EGFR interaction with the bisphosphonates or ApppI/ApppD. Representative correlations between the EGFR copy number and the increase in growth inhibition IC_{50} on GGOH addition for ibandronate, risedronate and pamidronate are shown in Figure 7b and Figure S18. Only very small rescue effects are found with pamidronate, consistent with earlier work[67] suggesting primary targets other than prenylation, for this bisphosphonate.

Taken together, the results discussed above indicate: First, NBPs do not significantly inhibit the EGFR. Second, there are no EGFR bisphosphonate-inhibition correlations with cell activity. Third, some kinases are inhibited by ApppI and ApppD, and cell growth inhibition correlates with ApppI levels, but kinase inhibition is weak, so the ANT is a likely target. Fourth, the correlation between cell growth inhibition and GGPPS inhibition reflects the importance of protein geranylgeranylation. Fifth, there are large increases in GGOH-rescue seen in high EGFR copy number cells, but since EGFR inhibition is so weak, this represents an indirect effect, due to the importance of protein prenylation and FPPS/GGPPS inhibition. Sixth, GGOH-rescues can have additional mechanisms of action beyond prenylation-rescue since the GGPP that is formed in cells from GGOH is a known inhibitor of mevalonate kinase, whose inhibition (together with HMGCoAR degradation) will lead to reduced ApppI/ApppD levels. In brief then, all of our results support the canonical prenylation+ANT mechanism of action for the NBPs and not the kinase-inhibition mechanism, although for the NNBPs, our results do support an ANT+kinase mechanism. There is, therefore, multi-targeting for both NBPs as well as NNBPs. Interestingly, "ApXpp" compounds (in which the Pα-O-Pβ bridging oxygen is replaced by e.g. CHF) have been reported to act as substrates for kinases such as EGFR and SRC,[68] the terminal Pβ-O-Pγ group still being capable of substrate phosphorylation. With X=CHF, there is remarkable ~1000x difference in activity between the R and S epimers, although activity was less than that found with ATP itself.[68] In the AppXp systems, the terminal Pβ-X-Pγ group is inactive, however, due to the presence of two P-C bonds, so these compounds can act as kinase inhibitors.

CONCLUSIONS

The results that we have presented above lead to some new views as to the mechanism of action of bisphosphonates. Historically, nitrogen-containing bisphosphonates (such as alendronate, ibandronate, risedronate and zoledronate) have all been thought to inhibit protein prenylation and via ApppI, the adenine nucleotide translocase with NNBPs (like clodronate or etidronate) producing other ATP-analogs, AppXp, that likewise target the ANT. More recently, however, a new mechanism of action of NBPs such as risedronate and zoledronate was proposed to involve direct inhibition of a kinase, the epidermal growth factor receptor or EGFR, but there were puzzling dose discrepancies between cell (~50 μM) and EGFR (~500 μM) inhibition by NBPs. We thus tested a broad range of NBPs against an expressed EGFR kinase domain that was potently inhibited by known kinase inhibitors finding very weak activity. We then hypothesized that since it bears strong structural similarity to ATP, the ApppI (and ApppD) that forms from the IPP/DMAPP which accumulates on FPPS inhibition might actually be targeting the EGFR. There was increased activity and this may contribute in some cases to NBP activity—albeit in a minor way. Remarkably, however, we then discovered that the ATP analogs that form with NNBPs, such as clodronate, were far more potent EGFR inhibitors than was ApppI— as well as potent inhibitors of other cell signaling kinases. Clodronate and its pre-prodrug forms, for example, are converted in cells to the ATP analog $AppCCl_2p$ that we find to be a low nM inhibitor of kinases such as PDGFRa, JAKs, and FGFR2, in addition to being an ANT inhibitor. Our 369-kinase kinome screen and dose-response results indicate that JAK3 is the kinase that is most potently inhibited by $AppCCl_2p$, of interest since JAK3 is the target for tofacitinib, a potent anti-inflammatory drug, and as discussed above, some NNBPs have anti-inflammatory activity. The JAK/STAT/Tyk2 pathways are targeted by cytokines and are involved in e.g. rheumatoid arthritis and of interest here, JAK3 and Tyk2 are inhibited by $AppCCl_2p$ (at 5 nM and ~230 nM, respectively, as is STAT3 phosphorylation (by **31**), suggesting a possible mechanism for clodronate (or its analogs) in blocking inflammation by targeting the JAK/STAT pathway. Our results also provide evidence that $AppCCl_2p$ targets tyrosine kinases (~78%) in preference to serine/threonine kinases, and the results of DFT and AIM theoretical calculations indicate stronger (~100x) hydrogen-bond interactions between $AppCCl_2p$ and Tyr *versus* with Ser/Thr. And finally, the observation that AppXp species are kinase inhibitors opens up new possibilities for the development of "pre-prodrugs" using the protecting groups (phosphoramidates, pivaloyloxymethylenes, isoproxils) used in antivirals to deliver otherwise highly polar species into cells, to be converted into novel, multi-target inhibitors.

EXPERIMENTAL SECTION

General information, experimental procedures, and characterization data are provided in the Supporting Information.

Supporting Information

Kinase inhibition assays. All kinase inhibition assays were carried out by the Reaction Biology Corporation (Malvern, PA) using their Kinase HotSpot℠ Profiling system. The base reaction buffers were typically 20 mM Hepes (pH 7.5), 10 mM $MgCl_2$, 1 mM EGTA, 0.02% Brij35, 0.02 mg/ml BSA, 0.1 mM Na_3VO_4, 2 mM DTT, 1% DMSO, and 1 μM ATP. IC_{50} values were extracted from 3x dilution 10-dose dose-response curves.

Cell growth inhibition by bisphosphonates. We used the methods described previously[13a,14,43] to determine cell growth inhibition by bisphosphonates, as well as cell growth inhibition rescues by GGOH. Cell line authentication was carried out in the Biopolymer/Genomics Core

Facility in the School of Medicine of the University of Maryland *via* short tandem repeat (STR) analysis using a Promega Geneprint 10 System.

AUTHOR INFORMATION

Corresponding Author

* E-mail: eo@chad.scs.uiuc.edu

Author Contributions

#These authors contributed equally

Author Information note

Current address: Xinxin Feng: Institute of Chemical Biology and Nanomedicine, State Key Laboratory of Chemo/Biosensing and Chemometrics, College of Chemistry and Chemical Engineering, Hunan University, Changsha, 410082, P.R. China

Notes

The authors declare no competing financial interest.

Funding Sources

This work was supported in part by the United States Public Health Service (National Institutes of Health Grants GM065307 and CA158191 to EO, and GM085774 to YZ), by a Harriet A. Harlin Professorship, by the University of Illinois Foundation/Oldfield Research Fund and by the Academy of Finland (Decision No. 292574 to PT).

ACKNOWLEDGMENT

We thank Jouko Vepsäläinen, Yoshimasa Tanaka, Eric Champagne, Javier Alguacil and Suzanne Peyrottes for providing ApppI samples; Yang Wang and Guodong Rao for helpful advice; Robert Gennis and Jefferson Chan for providing access to instrumentation, and Hong Chen for providing cells.

REFERENCES

1. Russell, R. G. G., Bisphosphonates: The first 40 years. *Bone* **2011,** *49* (1), 2-19.
2. Fleisch, H.; Russell, R. G.; Simpson, B.; Muhlbauer, R. C., Prevention by a diphosphonate of immobilization "osteoporosis" in rats. *Nature* **1969,** *223* (5202), 211-212.
3. Fleisch, H.; Russell, R. G.; Straumann, F., Effect of pyrophosphate on hydroxyapatite and its implications in calcium homeostasis. *Nature* **1966,** *212* (5065), 901-903.
4. Rogers, M. J.; Russell, R. G. G.; Blackburn, G. M.; Williamson, M. P.; Watts, D. J., Metabolism of halogenated bisphosphonates by the cellular slime mould *Dictyostelium discoideum*. *Biochem. Biophys. Res. Commun.* **1992,** *189* (1), 414-423.
5. Pelorgeas, S.; Martin, J.-B.; Satre, M., Cytotoxicity of dichloromethane diphosphonate and of 1-hydroxyethane-1,1-diphosphonate in the amoebae of the slime mould *Dictyostelium discoideum*: a ^{31}P NMR study. *Biochem. Pharmacol.* **1992,** *44* (11), 2157-2163.
6. Luckman, S. P.; Coxon, F. P.; Ebetino, F. H.; Russell, R. G.; Rogers, M. J., Heterocycle-containing bisphosphonates cause apoptosis and inhibit bone resorption by preventing protein prenylation: evidence from structure-activity relationships in J774 macrophages. *J. Bone Miner. Res.* **1998,** *13* (11), 1668-1678.
7. Luckman, S. P.; Hughes, D. E.; Coxon, F. P.; Graham, R.; Russell, G.; Rogers, M. J., Nitrogen-containing bisphosphonates inhibit the mevalonate pathway and prevent post-translational prenylation of GTP-binding proteins, including Ras. *J. Bone Miner. Res.* **1998,** *13* (4), 581-589.
8. Cromartie, T. H.; Fisher, K. J.; Grossman, J. N., The discovery of a novel site of action for herbicidal bisphosphonates. *Pest. Biochem. Physiol.* **1999,** *63* (2), 114-126.
9. van Beek, E.; Pieterman, E.; Cohen, L.; Löwik, C.; Papapoulos, S., Farnesyl pyrophosphate synthase is the molecular target of nitrogen-containing bisphosphonates. *Biochem. Biophys. Res. Commun.* **1999,** *264* (1), 108-111.
10. Martin, M. B.; Arnold, W.; Heath Iii, H. T.; Urbina, J. A.; Oldfield, E., Nitrogen-containing bisphosphonates as carbocation transition state analogs for isoprenoid biosynthesis. *Biochem. Biophys. Res. Commun.* **1999,** *263* (3), 754-758.
11. Keller, R. K.; Fliesler, S. J., Mechanism of aminobisphosphonate action: characterization of alendronate inhibition of the isoprenoid pathway. *Biochem. Biophys. Res. Commun.* **1999,** *266* (2), 560-563.
12. Bergstrom, J. D.; Bostedor, R. G.; Masarachia, P. J.; Reszka, A. A.; Rodan, G., Alendronate is a specific, nanomolar inhibitor of farnesyl diphosphate synthase. *Arch. Biochem. Biophys.* **2000,** *373* (1), 231-241.
13. Grove, J. E.; Brown, R. J.; Watts, D. J., The intracellular target for the antiresorptive aminobisphosphonate drugs in *Dictyostelium discoideum* is the enzyme farnesyl diphosphate synthase. *J. Bone Miner. Res.* **2000,** *15* (5), 971-981.
14. Lehenkari, P. P.; Kellinsalmi, M.; Näpänkangas, J. P.; Ylitalo, K. V.; Mönkkönen, J.; Rogers, M. J.; Azhayev, A.; Väänänen, H. K.; Hassinen, I. E., Further insight into mechanism of action of clodronate: inhibition of mitochondrial ADP/ATP translocase by a nonhydrolyzable, adenine-containing metabolite. *Mol. Pharmacol.* **2002,** *61* (5), 1255-1262.
15. Mönkkönen, H.; Auriola, S.; Lehenkari, P.; Kellinsalmi, M.; Hassinen, I. E.; Vepsäläinen, J.; Mönkkönen, J., A new endogenous ATP analog (ApppI) inhibits the mitochondrial adenine nucleotide translocase (ANT) and is responsible for the apoptosis induced by nitrogen-containing bisphosphonates. *Br. J. Pharmacol.* **2006,** *147* (4), 437-445.
16. Mönkkönen, H.; Kuokkanen, J.; Holen, I.; Evans, A.; Lefley, D. V.; Jauhiainen, M.; Auriola, S.; Mönkkönen, J., Bisphosphonate-induced ATP analog formation and its effect on inhibition of cancer cell growth. *Anti-Cancer Drugs* **2008,** *19* (4), 391-399.
17. Mitrofan, L. M.; Pelkonen, J.; Monkkonen, J., The level of ATP analog and isopentenyl pyrophosphate correlates with zoledronic acid-induced apoptosis in cancer cells in vitro. *Bone* **2009,** *45* (6), 1153-1160.
18. Adjuvant bisphosphonate treatment in early breast cancer: meta-analyses of individual patient data from randomised trials. *Early Breast Cancer Trialists'*

Collaborative Group (EBCTCG). Lancet **2015,** *386* (10001), 1353-1361.
19. Hadji, P.; Coleman, R. E.; Wilson, C.; Powles, T. J.; Clézardin, P.; Aapro, M.; Costa, L.; Body, J.-J.; Markopoulos, C.; Santini, D.; Diel, I.; Di Leo, A.; Cameron, D.; Dodwell, D.; Smith, I.; Gnant, M.; Gray, R.; Harbeck, N.; Thurlimann, B.; Untch, M.; Cortes, J.; Martin, M.; Albert, U.-S.; Conte, P.-F.; Ejlertsen, B.; Bergh, J.; Kaufmann, M.; Holen, I., Adjuvant bisphosphonates in early breast cancer: consensus guidance for clinical practice from a European panel. *Ann. Oncol.* **2015**, 27(3), 379-390.
20. Yuen, T.; Stachnik, A.; Iqbal, J.; Sgobba, M.; Gupta, Y.; Lu, P.; Colaianni, G.; Ji, Y.; Zhu, L.-L.; Kim, S.-M.; Li, J.; Liu, P.; Izadmehr, S.; Sangodkar, J.; Bailey, J.; Latif, Y.; Mujtaba, S.; Epstein, S.; Davies, T. F.; Bian, Z.; Zallone, A.; Aggarwal, A. K.; Haider, S.; New, M. I.; Sun, L.; Narla, G.; Zaidi, M., Bisphosphonates inactivate human EGFRs to exert antitumor actions. *Proc. Natl. Acad. Sci. U. S. A.* **2014,** *111* (50), 17989-17994.

21. Stachnik, A.; Yuen, T.; Iqbal, J.; Sgobba, M.; Gupta, Y.; Lu, P.; Colaianni, G.; Ji, Y.; Zhu, L. L.; Kim, S. M.; Li, J.; Liu, P.; Izadmehr, S.; Sangodkar, J.; Scherer, T.; Mujtaba, S.; Galsky, M.; Gomez, J.; Epstein, S.; Buettner, C.; Bian, Z.; Zallone, A.; Aggarwal, A. K.; Haider, S.; New, M. I.; Sun, L.; Narla, G.; Zaidi, M., Repurposing of bisphosphonates for the prevention and therapy of nonsmall cell lung and breast cancer. *Proc. Natl. Acad. Sci. U. S. A.* **2014,** *111* (50), 17995-8000.
22. Zhang, Y.; Leon, A.; Song, Y.; Studer, D.; Haase, C.; Koscielski, L. A.; Oldfield, E., Activity of nitrogen-containing and non-nitrogen-containing bisphosphonates on tumor cell lines. *J. Med. Chem.* **2006,** *49* (19), 5804-5814.
23. Webster, M. R.; Zhao, M.; Rudek, M. A.; Hann, C. L.; Freel Meyers, C. L., Bisphosphonamidate clodronate prodrug exhibits potent anticancer activity in non-small-cell lung cancer cells. *J. Med. Chem.* **2011,** *54* (19), 6647-6656.
24. Webster, M. R.; Kamat, C.; Connis, N.; Zhao, M.; Weeraratna, A. T.; Rudek, M. A.; Hann, C. L.; Freel Meyers, C. L., Bisphosphonamidate clodronate prodrug exhibits selective cytotoxic activity against melanoma cell lines. *Mol. Cancer Ther.* **2014,** *13* (2), 297-306.
25. Xia, Y.; Liu, Y.-L.; Xie, Y.; Zhu, W.; Guerra, F.; Shen, S.; Yeddula, N.; Fischer, W.; Low, W.; Zhou, X.; Zhang, Y.; Oldfield, E.; Verma, I. M., A combination therapy for KRAS-driven lung adenocarcinomas using lipophilic bisphosphonates and rapamycin. *Sci. Transl. Med.* **2014,** *6* (263), 263ra161.
26. Turhanen, P. A., Synthesis of a biologically important adenosine triphosphate analogue, ApppD. *ACS Omega* **2017,** *2* (6), 2835-2838.
27. Puljula, E.; Turhanen, P. A., Semi-preparative high-performance countercurrent chromatography method for the purification of chemically synthesized ATP analogue, ApppI. *J. Chromatogr. B* **2017,** *1063*, 180-182.
28. Yun, C. H.; Mengwasser, K. E.; Toms, A. V.; Woo, M. S.; Greulich, H.; Wong, K. K.; Meyerson, M.; Eck, M. J., The T790M mutation in EGFR kinase causes drug resistance by increasing the affinity for ATP. *Proc. Natl. Acad. Sci. U. S. A.* **2008,** *105* (6), 2070-2075.
29. Monkkonen, H.; Rogers, M. J.; Makkonen, N.; Niva, S.; Auriola, S.; Monkkonen, J., The cellular uptake and metabolism of clodronate in RAW 264 macrophages. *Pharm. Res.* **2001,** *18* (11), 1550-1555.
30. Wang, R.; Griffin, P. R.; Small, E. C.; Thompson, J. E., Mechanism of Janus kinase 3-catalyzed phosphorylation of a Janus kinase 1 activation loop peptide. *Arch. Biochem. Biophys.* **2003,** *410* (1), 7-15.
31. Junankar, S.; Shay, G.; Jurczyluk, J.; Ali, N.; Down, J.; Pocock, N.; Parker, A.; Nguyen, A.; Sun, S.; Kashemirov, B.; McKenna, C. E.; Croucher, P. I.; Swarbrick, A.; Weilbaecher, K.; Phan, T. G.; Rogers, M. J., Real-time intravital imaging establishes tumor-associated macrophages as the extraskeletal target of bisphosphonate action in cancer. *Cancer Discov.* **2015,** *5* (1), 35-42.
32. Joyce, J. A.; Pollard, J. W., Microenvironmental regulation of metastasis. *Nat. Rev. Cancer* **2009,** *9* (4), 239-252.
33. Bingle, L.; Brown, N. J.; Lewis, C. E., The role of tumour-associated macrophages in tumour progression: implications for new anticancer therapies. *J. Pathol.* **2002,** *196* (3), 254-265.
34. Raikkonen, J.; Crockett, J. C.; Rogers, M. J.; Monkkonen, H.; Auriola, S.; Monkkonen, J., Zoledronic acid induces formation of a pro-apoptotic ATP analogue and isopentenyl pyrophosphate in osteoclasts *in vivo* and in MCF-7 cells in vitro. *Br. J. Pharmacol.* **2009,** *157* (3), 427-435.
35. Monkkonen, J.; Simila, J.; Rogers, M. J., Effects of tiludronate and ibandronate on the secretion of proinflammatory cytokines and nitric oxide from macrophages *in vitro*. *Life Sci.* **1998,** *62* (8), PL95-102.
36. Cocco, R.; Tofi, C.; Fioravanti, A.; Nerucci, F.; Nannipieri, F.; Zampieri, A.; Rosini, S.; Marcolongo, R., Effects of clodronate on synovial fluid levels of some inflammatory mediators, after intra-articular administration to patients with synovitis secondary to knee osteoarthritis. *Boll. Soc. Ital. Biol. Sper.* **1999,** *75* (11-12), 71-76.
37. Rovetta, G.; Monteforte, P., Efficacy of disodium-clodronate in the management of joint pain in rheumatoid arthritis. Six months open study. *Minerva. Med.* **2003,** *94* (5), 353-357.
38. Wang, C. H.; Shen, Y. C.; Hsieh, J. J.; Yeh, K. Y.; Chang, J. W., Clodronate alleviates cachexia and prolongs survival in nude mice xenografted with an anaplastic thyroid carcinoma cell line. *J. Endocrinol.* **2006,** *190* (2), 415-423.
39. Rossini, M.; Viapiana, O.; Ramonda, R.; Bianchi, G.; Olivieri, I.; Lapadula, G.; Adami, S., Intra-articular clodronate for the treatment of knee osteoarthritis: dose ranging study vs hyaluronic acid. *Rheumatology (Oxford)* **2009,** *48* (7), 773-778.
40. Oizumi, T.; Yamaguchi, K.; Funayama, H.; Kuroishi, T.; Kawamura, H.; Sugawara, S.; Endo, Y., Necrotic actions of nitrogen-containing bisphosphonates and their inhibition by clodronate, a non-nitrogen-containing bisphosphonate in mice: potential for utilization of clodronate as a combination drug with a nitrogen-containing bisphosphonate. *Basic Clin. Pharmacol. Toxicol.* **2009,** *104* (5), 384-392.

41. Saviola, G.; Abdi-Ali, L.; Campostrini, L.; Sacco, S.; Baiardi, P.; Manfredi, M.; Mannoni, A.; Benucci, M., Clodronate and hydroxychloroquine in erosive osteoarthritis: a 24-month open randomized pilot study. *Mod. Rheumatol.* **2012,** *22* (2), 256-263.
42. Shima, K.; Tsuchiya, M.; Oizumi, T.; Takano-Yamamoto, T.; Sugawara, S.; Endo, Y., Inflammatory effects of nitrogen-containing bisphosphonates (N-BPs): modulation by non-N-BPs. *Biol. Pharm. Bull.* **2017,** *40* (1), 25-33.
43. Yamaoka, K., Janus kinase inhibitors for rheumatoid arthritis. *Curr. Opin. Chem. Biol.* **2016,** *32*, 29-33.
44. Winthrop, K. L., The emerging safety profile of JAK inhibitors in rheumatic disease. *Nat. Rev. Rheumatol.* **2017**, *13* (4), 234-243.
45. Rose, K.; Finger, I. E.; Ferenz, K. B., Interaction of clodronate with fibroblast growth factor 2 reduces FGF2-activity in endothelial cells. *Biomed. Pharmacother.* **2011,** *65* (1), 46-51.
46. Eid, S.; Turk, S.; Volkamer, A.; Rippmann, F.; Fulle, S., KinMap: a web-based tool for interactive navigation through human kinome data. *BMC Bioinformatics* **2017,** *18* (1), 16.
47. Li, J.; Feng, X.; Zhu, W.; Oskolkov, N.; Zhou, T.; Kim, B. K.; Baig, N.; McMahon, M. T.; Oldfield, E., Chemical exchange saturation transfer (CEST) agents: quantum chemistry and MRI. *Chemistry* **2016,** *22* (1), 264-271.
48. Bader, R. F. W., *Atoms in Molecules: A quantum Theory (International Series of Monographs on Chemisrty) 1st Edition* Clarendon Press, Oxford, **1994**.
49. Arnold, W. D.; Oldfield, E., The chemical nature of hydrogen bonding in proteins via NMR: J-couplings, chemical Shifts, and AIM theory. *J. Am. Chem. Soc.* **2000,** *122* (51), 12835-12841.
50. Bader, R. F. W., A bond path: a universal indicator of bonded interactions. *J. Phys. Chem. A* **1998,** *102* (37), 7314-7323.
51. Blackburn, G. M.; Kent, D. E.; Kolkmann, F., Three new [β],[γ]-methylene analogues of adenosine triphosphate. *J. C. S. Chem. Comm.* **1981,** (22), 1188-1190.
52. Reuben, J. S.; Dinh, L.; Lee, J.; Stateson, J.; Kamara, H.; Xiang, L.; Opperman, L. A., Bisphosphonates inhibit phosphorylation of signal transducer and activator of transcription 3 and expression of suppressor of cytokine signaling 3: implications for their effects on innate immune function and osteoclastogenesis. *Oral Surg. Oral Med. Oral Pathol. Oral Radiol. Endod* **2011,** *111* (2), 196-204.
53. Glantschnig, H.; Fisher, J. E.; Wesolowski, G.; Rodan, G. A.; Reszka, A. A., M-CSF, TNFalpha and RANK ligand promote osteoclast survival by signaling through mTOR/S6 kinase. *Cell Death Differ.* **2003,** *10* (10), 1165-1177.
54. Zhang, Y.; Cao, R.; Yin, F.; Hudock, M. P.; Guo, R.-T.; Krysiak, K.; Mukherjee, S.; Gao, Y.-G.; Robinson, H.; Song, Y.; No, J. H.; Bergan, K.; Leon, A.; Cass, L.; Goddard, A.; Chang, T.-K.; Lin, F.-Y.; Beek, E. V.; Papapoulos, S.; Wang, A. H. J.; Kubo, T.; Ochi, M.; Mukkamala, D.; Oldfield, E., Lipophilic bisphosphonates as dual farnesyl/geranylgeranyl diphosphate synthase inhibitors: an x-ray and NMR Investigation. *J. Am. Chem. Soc.* **2009,** *131* (14), 5153-5162.
55. Chen, C. K. M.; Hudock, M. P.; Zhang, Y.; Guo, R.-T.; Cao, R.; No, J. H.; Liang, P.-H.; Ko, T.-P.; Chang, T.-H.; Chang, S.-c.; Song, Y.; Axelson, J.; Kumar, A.; Wang, A. H. J.; Oldfield, E., Inhibition of geranylgeranyl diphosphate synthase by bisphosphonates: a crystallographic and computational investigation. *J. Med. Chem.* **2008,** *51* (18), 5594-5607.
56. Garza, R. M.; Tran, P. N.; Hampton, R. Y., Geranylgeranyl pyrophosphate is a potent regulator of HRD-dependent 3-Hydroxy-3-methylglutaryl-CoA reductase degradation in yeast. *J. Biol. Chem.* **2009,** *284* (51), 35368-35380.
57. Sever, N.; Song, B. L.; Yabe, D.; Goldstein, J. L.; Brown, M. S.; DeBose-Boyd, R. A., Insig-dependent ubiquitination and degradation of mammalian 3-hydroxy-3-methylglutaryl-CoA reductase stimulated by sterols and geranylgeraniol. *J. Biol. Chem.* **2003,** *278* (52), 52479-52490.
58. Hinson, D. D.; Chambliss, K. L.; Toth, M. J.; Tanaka, R. D.; Gibson, K. M., Post-translational regulation of mevalonate kinase by intermediates of the cholesterol and nonsterol isoprene biosynthetic pathways. *J. Lipid. Res.* **1997,** *38* (11), 2216-2223.
59. Fisher, J. E.; Rogers, M. J.; Halasy, J. M.; Luckman, S. P.; Hughes, D. E.; Masarachia, P. J.; Wesolowski, G.; Russell, R. G.; Rodan, G. A.; Reszka, A. A., Alendronate mechanism of action: geranylgeraniol, an intermediate in the mevalonate pathway, prevents inhibition of osteoclast formation, bone resorption, and kinase activation in vitro. *Proc. Natl. Acad. Sci. U. S. A.* **1999,** *96* (1), 133-138.
60. van beek, E.; Lowik, C.; van der Pluijm, G.; Papapoulos, S., The role of geranylgeranylation in bone resorption and its suppression by bisphosphonates in fetal bone explants in vitro: A clue to the mechanism of action of nitrogen-containing bisphosphonates. *J. Bone Miner. Res.* **1999,** *14* (5), 722-729.
61. Goffinet, M.; Thoulouzan, M.; Pradines, A.; Lajoie-Mazenc, I.; Weinbaum, C.; Faye, J. C.; Seronie-Vivien, S., Zoledronic acid treatment impairs protein geranyl-geranylation for biological effects in prostatic cells. *BMC Cancer* **2006,** *6*, 60.
62. Coxon, F. P.; Helfrich, M. H.; Van't Hof, R.; Sebti, S.; Ralston, S. H.; Hamilton, A.; Rogers, M. J., Protein geranylgeranylation is required for osteoclast formation, function, and survival: inhibition by bisphosphonates and GGTI-298. *J. Bone Miner. Res.* **2000,** *15* (8), 1467-1476.
63. Zhang, G. H.; Cai, L. J.; Wang, Y. F.; Zhou, Y. H.; An, Y. F.; Liu, Y. C.; Peng, Y.; Chen, Z. F.; Liang, H., Novel compound PS-101 exhibits selective inhibition in non-small-cell lung cancer cell by blocking the EGFR-driven antiapoptotic pathway. *Biochem. Pharmacol.* **2013,** *86* (12), 1721-1730.
64. Van Schaeybroeck, S.; Kyula, J.; Kelly, D. M.; Karaiskou-McCaul, A.; Stokesberry, S. A.; Van Cutsem, E.; Longley, D. B.; Johnston, P. G., Chemotherapy-induced epidermal growth factor receptor activation determines response to combined gefitinib/chemotherapy treatment in non-small cell lung cancer cells. *Mol. Cancer Ther.* **2006,** *5* (5), 1154-1165.
65. Zhang, X. T.; Kang, L. G.; Ding, L.; Vranic, S.; Gatalica, Z.; Wang, Z. Y., A positive feedback loop of ER-alpha36/EGFR promotes malignant growth of ER-negative breast cancer cells. *Oncogene* **2011,** *30* (7), 770-780.

66. Goetz, M.; Ziebart, A.; Foersch, S.; Vieth, M.; Waldner, M. J.; Delaney, P.; Galle, P. R.; Neurath, M. F.; Kiesslich, R., *In vivo* molecular imaging of colorectal cancer with confocal endomicroscopy by targeting epidermal growth factor receptor. *Gastroenterology* **2010,** *138* (2), 435-446.
67. van Beek, E. R.; Cohen, L. H.; Leroy, I. M.; Ebetino, F. H.; Löwik, C. W. G. M.; Papapoulos, S. E., Differentiating the mechanisms of antiresorptive action of nitrogen containing bisphosphonates. *Bone* **2003,** *33* (5), 805-811.
68. Ni, F.; Kung, A.; Duan, Y.; Shah, V.; Amador, C. D.; Guo, M.; Fan, X.; Chen, L.; Chen, Y.; McKenna, C. E.; Zhang, C., Remarkably stereospecific utilization of ATP α,β-halomethylene analogues by protein kinases. *J. Am. Chem. Soc.* **2017,** *139* (23), 7701-7704.

TOC